Effects of Temperature and Viscosity on R67 Dihydrofolate Reductase Catalysis†

Shaileja Chopra, Rachel Lynch, Su-Hwa Kim, Michael Jackson, and Elizabeth E. Howell*,†

Department of Biochemistry, Cellular, and Molecular Biology, University of Tennessee, Knoxville, Tennessee 37996-0840

Received December 8, 2005; Revised Manuscript Received March 30, 2006

ABSTRACT: R67 dihydrofolate reductase (DHFR) is a novel homotetrameric protein that possesses 222 symmetry and a single, voluminous active site pore. This symmetry poses numerous limitations on catalysis; for example, two dihydrofolate (DHF) molecules or two NADPH molecules, or one substrate plus one cofactor can bind. Only the latter combination leads to catalysis. To garner additional information on how this enzyme facilitates transition-state formation, the temperature dependence of binding and catalysis was monitored. The binding of NADPH and DHF is enthalpy-driven. Previous primary isotope effect studies indicate hydride transfer is at least partially rate-determining. Accordingly, the activation energy associated with transition-state formation was measured and is found to be 6.9 kcal/mol ($\Delta H^{\ddagger}_{25} = 6.3$ kcal/mol). A large entropic component is also found associated with catalysis, $T\Delta S^{\ddagger}_{25} = -11.3$ kcal/mol. The poor substrate, dihydropteroate, binds more weakly than dihydrofolate ($\Delta\Delta G = 1.4$ kcal/mol) and displays a large loss in the binding enthalpy value ($\Delta\Delta H = 3.8$ kcal/mol). The k_{cat} value for dihydropteroate reduction is decreased 1600-fold compared to DHF usage. This effect appears to derive mostly from the $\Delta\Delta H$ difference in binding, demonstrating that the glutamate tail is important for catalysis. This result is surprising, as the *para*-aminobenzoyl-glutamate tail of DHF has been previously shown to be disordered by both NMR and crystallography studies. Viscosity studies were also performed and confirmed that the hydride transfer rate is not sensitive to sucrose addition. Surprisingly, binding of DHF, by both K_m and K_d determination, was found to be sensitive to added viscogens, suggesting a role for water in DHF binding.

Dihydrofolate reductase (EC 1.5.1.3) (DHFR) catalyzes the reduction of dihydrofolate (DHF)[1] to tetrahydrofolate (THF) using NADPH as a cofactor. Two different protein scaffolds that catalyze the DHFR reaction have been identified. The first corresponds to chromosomal *Escherichia coli* DHFR, which is the target of the antibacterial drug, trimethoprim (TMP). The second DHFR is encoded by an R-plasmid, which provides resistance to TMP. R67 DHFR is unrelated genetically and structurally to chromosomal DHFR. Chromosomal *E. coli* DHFR has been described as a well-evolved enzyme with an efficiency of 0.15 (*3*), while R67 DHFR has been suggested to be a model for a "primitive" enzyme that has not yet been optimized by evolution (*4*, *5*).

The proposal that R67 DHFR is a primitive enzyme arises from the constraints imposed by its structure coupled with its use of two substrates (dihydrofolate and NADPH). As shown in Figure 1, R67 DHFR is a homotetramer with a single active site pore that is solvent-accessible, except perhaps at the hourglass center when ligands are bound. The overall structure possesses 222 symmetry (*4*). The obligatory symmetry of the active site results in overlapping binding sites for DHF and NADPH. This can be seen experimentally, as R67 DHFR binds a total of two ligands; either two NADPH molecules or two folate/DHF molecules, or one NADPH plus one folate/DHF molecule (*6*). The first two complexes are dead-end complexes, while the third is the productive catalytic complex (see Figure 1 for a model). The ability to discriminate between the homoligand and heteroligand complexes mostly appears to arise from stacking between the ligands, as well as some contribution from the enzyme (*7*, *8*). It has been found experimentally that the greater the enthalpy change associated with formation of the productive ternary complex, the greater the catalytic efficiency (*9*). Other groups have correlated enthalpic effects with structural tightness (*10*−*12*). Another consequence arising from this particular constellation of structural features is that introduction of a mutation in the gene results in four mutations per active site. These mutations typically have large cumulative effects (*9*, *13*) and make it unlikely that R67 DHFR uses a general acid in its active site to facilitate catalysis (as addition of one general acid per gene will result in four general acids per active site pore). Rather, preprotonated DHF from solution is used as substrate (*14*). Finally, NADPD isotope effects using an H62C mutant of

† This work was supported by NSF Grant MCB-0445728.

* Corresponding author. Elizabeth E. Howell, Department of Biochemistry, Cellular & Molecular Biology, University of Tennessee, Knoxville, TN 37996-0840. Phone, 865-974-4507; fax, 865-974-6306; e-mail, lzh@utk.edu.

[1] Abbreviations: R67 DHFR, R67 dihydrofolate reductase; DHF, dihydrofolate; ITC, isothermal titration calorimetry; NADP(+/H), nicotinamide adenine dinucleotide phosphate (oxidized/reduced); pABA-glu, *para*-aminobenzoylglutamate tail of dihydrofolate/folate; wt, wild-type; MTA buffer, 100 mM Tris, 50 mM MES, 50 mM acetic acid polybuffer; ρ, density; η, viscosity; η/ρ, kinematic viscosity. This enzyme is a homotetramer, when a single residue is mentioned; all four related residues are implied.

10.1021/bi052504l CCC: $33.50
Published on Web 05/05/2006

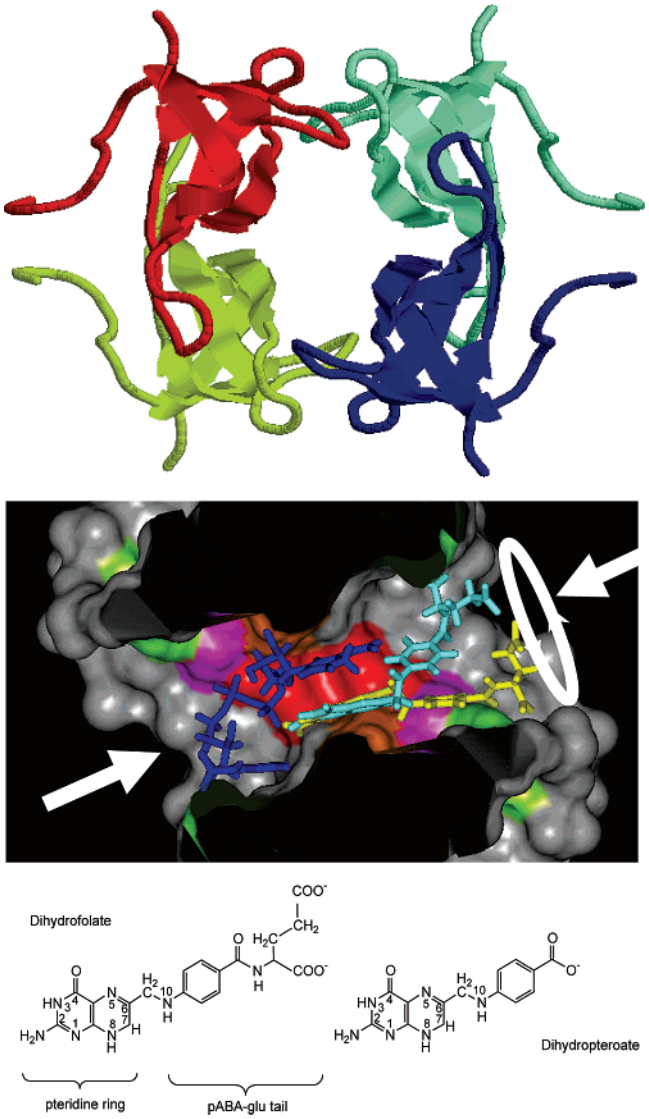

FIGURE 1: Structures of R67 DHFR, dihydrofolate, dihydropteroate, and a model of the productive ternary complex. The top panel shows the ribbon structure of R67 DHFR (protein data bank file 1VIE; (*4*)). The enzyme is a dimer of dimers; the monomer−monomer interfaces occur on the sides of the structure (sea green + blue or chartreuse + red), while the dimer−dimer interfaces occur on the top and bottom of the structure (sea green + red or chartreuse + blue). The active site pore corresponds to the "doughnut hole" in the center. The center panel shows a Connolly surface that is related to the structure shown in the top panel by a 90° rotation along the *y*-axis along with deletion of the symmetry-related dimer. This section describes the pore surface corresponding to the chartreuse and red monomers in the top panel. Arrows on opposite sides of the pore indicate where the ligands NADPH (blue) and folate (two possible docked conformers in cyan and yellow; (*22*)) can enter and orient at the center of the pore. The pteridine ring of folate has a fixed orientation near the center of the pore, while the *para*-aminobenzoylglutamate tail can adopt different conformations (as shown by the circular arrow), suggesting alternate interactions with lysine 32 residues (green) on either side of the pore. Also shown are the isoleucine 68 (red), glutamine 67 (orange), and tyrosine 69 (magenta) residues that line the active site pore forming key contacts with NADPH and folate. The bottom panel shows the DHF and DHP structures with atom labels from N1 to N10.

R67 DHFR find ^{D}V (= k_{cat} using NADPH/k_{cat} using NADPD) at pH 5.0 equals 3.6 ± 0.45, and at pH 7.0, ^{D}V = 3.3 ± 0.33 (*14*). These results indicate hydride transfer is at least partially rate-determining from pH 5−7.

While the 222 symmetry restricts the catalytic strategy of R67 DHFR, there are some advantages associated with this symmetry. The first positive feature is expenditure of less energy and DNA in encoding the genetic information. A second advantage pertains to the consequences of symmetry breaking, whereby different properties and packing relationships arise (*15*, *16*). For example, the initial binding of NADPH to R67 DHFR utilizes the symmetry of the protein by allowing binding to 1 of 4 symmetry-related sites. Once bound, NADPH creates a local asymmetric environment in the active site pore, which results in negative cooperativity disfavoring binding of a second NADPH molecule or positive cooperativity favoring binding of DHF (*6*). Both these cooperativity patterns strongly favor channeling of the binding pathway towards the productive ternary complex, NADPH·DHF. A third benefit of symmetry is the potential for multivalent binding (*17*). Here, once a site is occupied, the proximity of other symmetry-related sites can enhance binding by reduction of the associated entropy and/or by decreasing the dissociation rate (*18*, *19*). This type of effect appears likely to occur in R67 DHFR (*20*, *21*).

A study of the transition state used by R67 DHFR will help further deconvolute its catalytic strategy. From interligand NOEs using NMR, the bound $NADP^+$·folate complex is most consistent with use of an *endo* transition state, where the nicotinamide ring of cofactor overlaps that of the N5-containing pteridine ring of substrate (*7*, *22*). The *endo* transition state has been proposed to be 2 kcal/mol more stable than the *exo* transition state used by chromosomal *E. coli* DHFR (*23*, *24*). To garner more information concerning the transition state and mechanism used by R67 DHFR, temperature and viscosity effects were studied.

MATERIALS AND METHODS

Protein Purification. R67 DHFR was expressed in *E. coli* SK383 cells in TB media (*25*) containing 200 μg/mL ampicillin and 20 μg/mL trimethoprim as previously described (*26*). Briefly, ammonium sulfate precipitation and ion-exchange column chromatography were used to purify the protein to homogeneity. Purified samples were dialyzed against distilled, deionized H_2O and then lyophilized. Protein concentrations were determined with a biuret assay (*27*).

Fluorescence Quenching. Binding of NADPH to 2.0 μM R67 DHFR was monitored at pH 7.0 in MTA buffer at various temperatures using tryptophan fluorescence as per Zhuang et al. (*28*). MTA is a polybuffer containing 50 mM MES, 100 mM Tris, and 50 mM acetic acid which maintains a constant ionic strength from pH 4.5−9.5 (*29*). Data were fit to

$$\mathrm{Fl} = F_o - 0.5F_o[P_{tot} + K_d + L_{tot} - [(P_{tot} + K_d + L_{tot})^2 - 4P_{tot}L_{tot}]^{1/2}] \quad (1)$$

where Fl is the observed fluorescence; L_{tot} is the total ligand concentration; and P_{tot}, K_d, and F_o are variables describing the number of enzyme binding sites, dissociation constant, and fluorescence yield per unit concentration of enzyme, respectively (*30*).

Steady-State Kinetics. Steady-state kinetic data were obtained using either a Perkin-Elmer λ3a or a λ35 spectro-

photometer interfaced with an IBM PS2 as previously described (*31*). Briefly, assays were performed at 30 °C in MTA polybuffer, by the addition of substrate (DHF) and cofactor (NADPH), followed by the addition of enzyme to initiate the reaction. To obtain k_{cat} and K_m values, the concentration of NADPH was held constant at a subsaturating level, while the concentration of DHF was varied. This process was repeated using four additional subsaturating concentrations of NADPH. The data were fit globally to the nonlinear bisubstrate Michaelis−Menten equation utilizing SAS (statistical analysis software; (*8*, *32*)). The NLINEK macro for use in SAS is available at http://animalscience.ag.utk.edu/faculty/saxton/software.htm.

The temperature dependence of the steady-state kinetic behavior of R67 DHFR was studied from 20 to 50°C. The pH meter was standardized at each temperature and MTA buffer titrated to pH 7.0. Within error, the extinction coefficient of the reaction did not change as temperature was varied (data not shown).

For solutions containing viscogens, the steady-state data were initially monitored as described above. When it became apparent that the main variation occurred in the K_m for DHF, data were then collected using saturating NADPH concentrations.

Reduction of the alternate substrate, dihydropteroic acid (DHP), was also studied. Pteroic acid was purchased from Schircks Laboratories and reduced to DHP according to Prabhu et al. (*33*). NMR analysis confirmed formation of the reduced species and the simultaneous disappearance of the oxidized compound. The molar extinction coefficient used to assess reduction of DHP was monitored and found to be the same as for DHF reduction, which is 12 300 L M^{-1} cm^{-1} (*34*). Since this is a poor substrate, higher enzyme concentrations were used, and Michaelis−Menten conditions did not apply. Data were fit to eq 2

$$v = \frac{k_{cat}([E_{tot}] + [S_{tot}] + K_d) - \{([E_{tot}] + [S_{tot}] + K_d)^2 - 4[E_{tot}][S_{tot}]\}^{1/2}}{2} \quad (2)$$

where $[E_{tot}]$, $[S_{tot}]$, K_d, v, and k_{cat} are the total enzyme and substrate concentrations, the substrate binding constant, the initial velocity, and the catalytic rate constant, respectively (*35*).

Determination of Substrate pK_a Values. The pK_a value for the N5 atom in DHF was determined as per Maharaj et al. (*36*). Essentially, the absorbance of a DHF solution (<30 μM) was monitored within 30 s at 228 nm. A range of pH values were obtained using 0.2 M sodium phosphate buffer or various concentrations of HCl (<0.25 M). To minimize any precipitation of DHF near its isoelectric point, DHF was dissolved first, followed by addition of buffer or HCl. Titrations were performed at 10, 15, and 20 °C. The data were fit to an equation describing a standard ionization curve (*37*). An identical approach was used to determine the N5 pK_a of dihydropteroic acid.

Viscosity Measurements. Kinematic viscosity (η/ρ in mm^2/s) was monitored using a Cannon-Fenske viscometer equilibrated at 30 °C in a Precision Temp-Trol mineral oil bath. Kinematic viscosity was converted to viscosity (η) by multiplying by the density of the solution (ρ in g/mL). Sucrose (≤1.75 M) was added to increase η to ≤10.5 cP. Relative viscosities (η/η_o) were calculated using MTA buffer as the reference. Trehalose (≤1.6 M), also a disaccharide, was additionally used as a viscogen to determine whether sucrose had a specific or nonspecific effect.

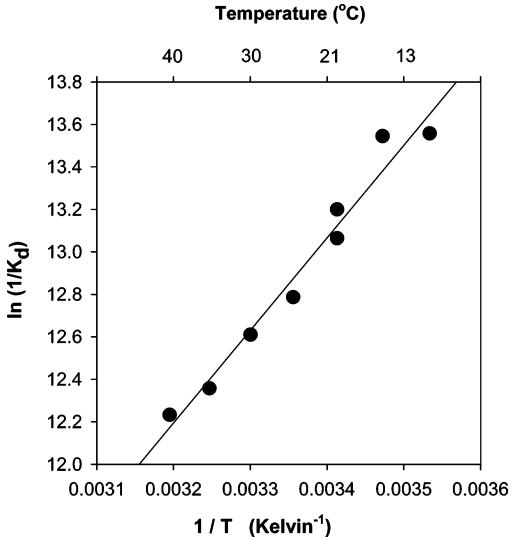

FIGURE 2: A van't Hoff plot describing the temperature dependence of NADPH binding to R67 DHFR. Binding of NADPH was monitored by fluorescence quenching, which only describes titration of a single NADPH molecule. Errors associated with the K_d values are smaller than the symbol size. Best-fit values are given in the text, as well as in Table 2.

Isothermal Titration Calorimetry. Affinities and stoichiometries, as well as ΔH values, were determined for binding studies using isothermal titration calorimetry (ITC) as previously described (*6*). Measurements were performed on a VP-ITC microcalorimeter from MicroCal interfaced to a Gateway PC for data acquisition and analysis. Origin v.5 scientific software was used to analyze the data. The design and use of this instrument have been previously described (*38*). R67 DHFR concentrations typically ranged between 60 and 150 μM in MTA buffer (pH 8). Experiments were performed at least in duplicate. For titrations with sucrose present, MTA buffer plus sucrose was used in the reference cell.

RESULTS

What Is the Temperature Dependence of NADPH Binding to R67 DHFR? To determine the temperature dependence of the K_d for NADPH, a fluorescence-quenching approach was employed. Titration of NADPH into R67 DHFR was performed at a constant temperature, and the data were fit to obtain a K_d value. Dissociation constants were obtained from 10 to 40 °C. As the temperature rose, so did the K_d. The data were then analyzed using the van't Hoff equation:

$$\ln K_a = (-\Delta H/RT) + \Delta S/R \quad (3)$$

where the association constant, K_a, equals $1/K_d$, ΔH is the enthalpy change, ΔS is the entropy change, R is the gas constant, and T is the temperature in degrees Kelvin. Figure 2 shows the resulting plot. The slope of these plots equals $-\Delta H/R$, and ΔH is calculated to be -8.6 ± 0.6 kcal/mol. The linear nature of the plot predicts that the enthalpy change for complex formation will be independent of temperature

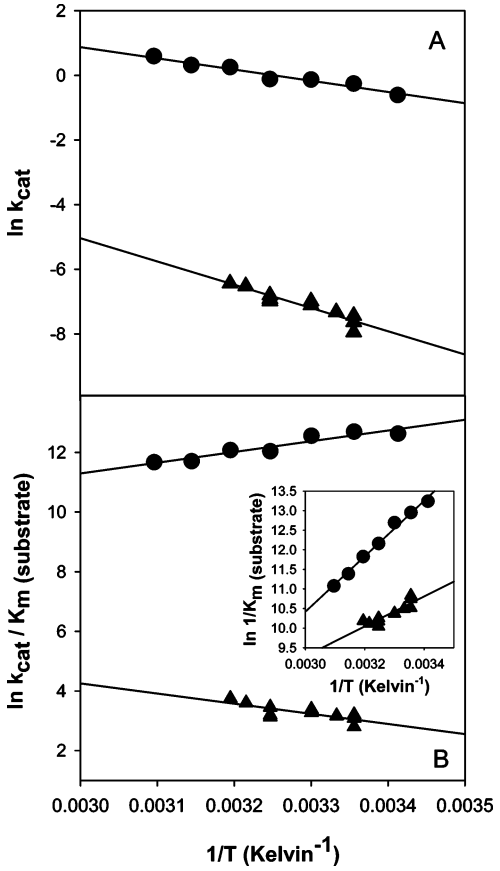

FIGURE 3: Arrhenius plots describing R67 DHFR catalysis. Steady-state kinetic analysis was performed as described in Materials and Methods. Reduction of DHF and DHP were both studied and are described by ● and ▲ points, respectively. Errors associated with the various parameters are smaller than the symbol size. Panel A describes the ln k_{cat} values, while panel B describes ln $k_{cat}/K_{m(substrate)}$ data. The inset plots the variance of ln $1/K_{m(substrate)}$ with inverse temperature.

within the range studied (10−40 °C), with a heat capacity change (ΔC_p) near zero (*39*, *40*).

What Is the Temperature Dependence of R67 DHFR Catalysis? The steady-state kinetic behavior of R67 DHFR was also studied and found to be dependent on temperature from 20 to 50 °C. Effects on both k_{cat} and K_m values were observed. The data were then analyzed using the Arrhenius equation:

$$k_{cat} = Ae^{-E_a/RT} \quad (4)$$

where k is the rate, A is the pre-exponential factor, and E_a is the activation energy (*41*). Figure 3 plots the reciprocal temperature versus ln k_{cat}, as well as ln $k_{cat}/K_{m\ (DHF)}$. The plots are linear, consistent with a single rate-determining step being monitored. The slope for this plot corresponds to E_a/R, where E_a is the activation energy for the reaction. For the k_{cat} plot, E_a is calculated[2] to be 6.90 ± 0.6 kcal/mol. From the equation $\Delta H^{\ddagger} = E_a - RT$, $\Delta H^{\ddagger}_{25}$ for R67 DHFR can be calculated as 6.3 ± 0.6 kcal/mol, and from $\Delta G^{\ddagger} = -RT \ln(k_{cat}h/k_BT)$, $\Delta G^{\ddagger}_{25}$ can be calculated as 17.6 ± 0.1 kcal/mol (where h is Planck's constant and k_B is the Boltzmann constant) (*42*, *43*). $T\Delta S^{\ddagger}_{25}$ can then be computed as −11.3 ± 0.6 kcal/mol from $\Delta G^{\ddagger} = \Delta H^{\ddagger} - T\Delta S^{\ddagger}$.

Temperature Dependence of the N5 pK_a in DHF. Since the pH at which our assays are performed does not occur at a plateau in the pH profile for R67 DHFR and as this enzyme reduces pre-protonated DHF (*14*), we also determined how temperature would affect the N5 pK_a of DHF. The structure of the substrate, DHF, is given in Figure 1 along with atom labels. To obtain thermodynamic values associated with N5 protonation, this pK_a was monitored as a function of temperature. While previous studies of organic cyclic compounds predict that the N5 pK_a should decrease with increasing temperature (*44*), the N5 titration in DHF was directly monitored from 10 to 20 °C. A typical titration curve is given in Supporting Information. Above 20 °C, DHF is not sufficiently stable in acidic solutions to continue the titrations (*36*); however, the general trend of a decreased pK_a associated with the N5 atom can be observed with increasing temperature. Specifically, at 10 °C, the N5 pK_a is 2.86 ± 0.01, while at 15 °C, the pK_a is 2.74 ± 0.03, and at 20 °C, the pK_a is 2.69 ± 0.02. These values compare with an N5 pK_a equal to 2.59, previously obtained at 20 °C (*36*).

Are There Any Viscosity Effects on k_{cat}/K_m? A common approach to show that the rate of the enzyme under study is not limited by either binding or release of ligands involves monitoring the steady-state rate in solutions of varying viscosities. If ligand binding is the rate-determining step, increasing the microscopic viscosity will decrease k_{cat}/K_m in a linear fashion (*45*, *46*). Enzymes possessing diffusion-limited rates typically display k_{cat}/K_m values of 10^7-10^8 M^{-1} s^{-1} (*47*). Since the $k_{cat}/K_{m(DHF)}$ value for R67 DHFR is only 3.2×10^5 M^{-1} s^{-1}, our initial expectation was that binding would not be rate-limiting. Also, the previous observation of NADPD isotope effects for our H62C mutant in R67 DHFR ($^DV = 3.3 \pm 0.33$ and $^DV/K_{m(DHF)} = 2.7 \pm 0.34$) suggested that hydride transfer is at least partially rate-limiting at pH 7 under both saturating and nonsaturating substrate conditions (*14*). To address these issues experimentally, we monitored catalysis in increasing concentrations of sucrose. No effect on k_{cat} was observed, consistent with product release not being rate-determining. Surprisingly, clear effects on $k_{cat}/K_{m(DHF)}$ were seen, as well as a small effect on $k_{cat}/K_{m(NADPH)}$ (~2-fold at the highest viscosity). The results are plotted in Figure 4. Viscogens can have a variety of effects, including perturbation of solvent structure. Since the viscogenic effect is predominately observed on $k_{cat}/K_{m(DHF)}$, a possibility is that the viscogen affects the water structure, which selectively affects DHF binding. Thus, the lower value of $k_{cat}/K_{m(DHF)}$ for R67 DHFR may describe a rate partially limited by productive enzyme−water−substrate association. Previous examples of enzymes with low k_{cat}/K_m values that are at least partially diffusion-controlled include chorismate mutase from *Bacillus subtilis* and ACC synthase (*48*, *49*).

To investigate whether sucrose acts specifically or whether it acts nonspecifically as a viscogen, trehalose was also used to alter the solution viscosity. At comparable relative viscosities (η/η_o), similar kinetic effects were observed using

[2] Alternate fits were also employed and provided similar values. To minimize error propagation, the raw data were also fit directly to rate $= Ae^{(-E_a/RT)}$. For this nonlinear fit, $E_a = 7.1 \pm 0.7$ kcal/mol and $\Delta H^{\ddagger}_{25} = 6.5 \pm 0.7$ kcal/mol. An Eyring plot ($1/T$ vs $\ln(kh/k_BT)$) was also used to evaluate $\Delta H^{\ddagger}$ and $\Delta S^{\ddagger}$ values, as the slope of this plot equals $\Delta H^{\ddagger}/R$ and the y-intercept equals $\Delta S^{\ddagger}/R$ (*1*). For DHF reduction, $\Delta H^{\ddagger} = 6.3 \pm 0.6$ kcal/mol and $T\Delta S^{\ddagger}_{25} = -11.8 \pm 0.6$ kcal/mol.

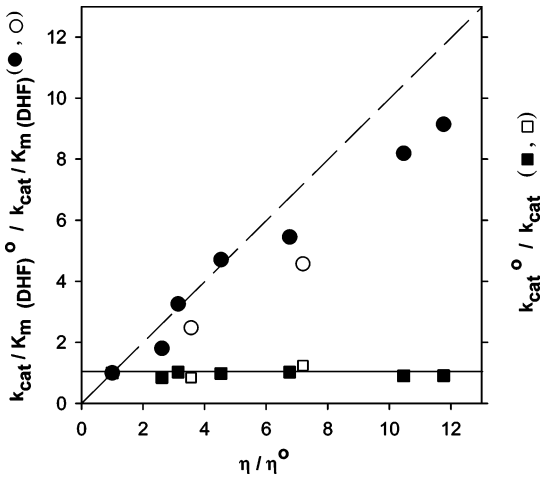

FIGURE 4: A plot of relative viscosity versus reciprocal relative k_{cat} and $k_{cat}/K_{m(DHF)}$ values. Relative viscosities (η/η_o) were calculated using MTA buffer as the reference (η_o). Reciprocal relative k_{cat} (squares) and $k_{cat}/K_{m(DHF)}$ (circles) values use steady-state kinetic values in MTA buffer as the reference. Data using sucrose or trehalose as the viscogen are represented by the filled (●, ■) and open (○, □) data points, respectively. A theoretical dashed line is shown with a slope of 1, consistent with diffusion being the rate-limiting process for k_{cat}/K_m. The solid line displays a slope of 0; the expected trend if diffusion did not have any effect on catalysis.

Table 1: Formation of the Ternary R67 DHFR·NADP$^+$·DHF Complex As Monitored by Isothermal Titration Calorimetry[a]

condition	K_d (μM)	ΔH (kcal/mol)	stoichiometry
MTA buffer	1.6 ± 0.1	−13.3 ± 0.8	0.85 ± 0.01
MTA buffer + 0.75 M sucrose ($\eta/\eta_o = 2.0$)	3.7 ± 0.2	−12.8 ± 1.0	1.1 ± 0.1
MTA buffer + 1.25 M sucrose ($\eta/\eta_o = 5.1$)	6.0 ± 0.4	−11.3 ± 1.3	1.0 ± 0.1

[a] DHF was titrated into a 1:3.5 (to 1:4) mixture of R67 DHFR:NADP$^+$ at a pH of 8.0 and 25 °C as previously described (*6*). The protein concentration ranged from 89 to 130 μM. ITC experiments were performed at pH 8 rather than pH 7 to minimize any contribution to the enthalpy change from the pH-dependent tetramer to 2 dimers dissociation (*2*).

either trehalose or sucrose (see Figure 4), consistent with viscosity being the primary variable.

To monitor the effect of viscosity on $K_{d(DHF)}$ directly, binding of DHF to R67 DHFR·NADP$^+$ was studied in increasing concentrations of sucrose using isothermal titration calorimetry. Table 1 lists the observed values, and a representative titration is available in Supporting Information. An approximately 4-fold increase in K_d was observed in buffer containing 1.25 M sucrose ($\eta/\eta_o = 5.1$). A clear effect on K_d is observed (including data obtained at 28 and 30 °C, not shown); however, as the η/η_o ratio rises, the ratio between the K_m and K_d values increases (from 2- to 3-fold). Values are not reported using even higher sucrose concentrations as the observed binding stoichiometry was affected. This may have resulted from any effects of higher mixing rates on protein stability or perhaps secondary effects on NADP$^+$ binding.

Use of Dihydropteroate as an Alternate Substrate. The temperature dependence of dihydropteroate (DHP) reduction was additionally studied. DHP is a fragment of DHF where a *para*-amino-benzoate tail replaces the *p*-aminobenzoyl-glutamate (pABA-glu) tail of DHF (see Figure 1). This fragment diminishes the negative charge to −1 and places the charge at a different position on the tail. DHP reduction is much slower than DHF reduction, with a k_{cat} value of (4.9 ± 0.17) × 10^{-4} s^{-1} and a $K_{m(DHP)}$ value of 23 ± 2.4 μM at 25 °C. These changes reflect an ~10-fold increase in K_m and an ~1600-fold decrease in k_{cat} with respect to DHF reduction. The temperature dependence of DHP reduction is also shown in Figure 3. The corresponding activation energy[3] is 14.3 ± 1.4 kcal/mol. $\Delta H^{\ddagger}_{25}$ can then be calculated as 13.7 ± 1.4 kcal/mol with a $\Delta G^{\ddagger}_{25}$ of 22 ± 0.1 kcal/mol and a $T\Delta S^{\ddagger}_{25}$ of −8.3 ± 1.4 kcal/mol. The various thermodynamic values comparing DHF versus DHP binding and catalysis are given in Table 2. To determine whether the reduction in catalytic rate could arise partly from a decrease in the N5 pK_a of DHP, a spectrophotometric titration was performed as described above for DHF (*36*). The N5 pK_a for DHP is 2.54 ± 0.03 at 20 °C, indicating no to minimal change in this pK_a compared to DHF.

DISCUSSION

Role of Water. No effects on k_{cat} were observed in our viscosity studies, consistent with hydride transfer being at least partially rate-determining. However, an effect was observed on the K_m for DHF with added sucrose or trehalose. To determine if the K_d for DHF was also affected, ITC studies were also performed. At low viscosities, $K_{d(DHF)}$ did increase with increasing viscosity and $K_{m(DHF)}$ approximated $K_{d(DHF)}$ (within a factor of 2). However, as the relative viscosity increased to 5.1, a greater divergence was noted between K_d and K_m (~3-fold), suggesting that the DHF K_m may contain some kinetic terms at higher viscosities.

If water is involved in a binding interaction, perturbation of water content should alter binding. For example, closer contact distances typically exclude water. In binding of ferredoxin to ferredoxin:NADP$^+$ reductase, Jelesarov and Bosshard (*50*) found increasing concentrations of glycerol resulted in tighter binding. They interpreted this behavior as arising from dehydration of the protein−protein interface, which led to tighter binding as water was released. For R67 DHFR, the opposite behavior has been observed, that is, weaker binding in increasing sucrose concentrations, suggesting water stabilizes DHF binding. This observation is consistent with previous NMR and crystallography studies, which have found the pABA-glu tail of DHF/folate is disordered when bound (*4*, *7*). Also, docking studies predicted the pABA-glu tail could interact with either symmetry-related K32 residue in one-half of the pore (*22*, *51*). Finally, addition of two asymmetric K32M mutations on opposite sides of the pore can have two topologies; that is, they can occur on the same dimer−dimer interface or they can exist diagonally on both dimer−dimer interfaces (see Figure 1 in ref *20*). These two asymmetric K32M double mutant topologies have been constructed and found to have similar effects on steady-state kinetic values. If a preferred topology

[3] Alternate fits were also employed for DHP reduction and, within error, were found to provide similar values. For a nonlinear fit to the equation: rate = $Ae^{(-E_a/RT)}$, E_a = 10.7 ± 1.8 kcal/mol and $\Delta H^{\ddagger}_{25}$ = 10.1 ± 1.8 kcal/mol. When an Eyring plot (1/T vs ln(kh/k_BT)) was used, $\Delta H^{\ddagger}$ was found to be 13.7 ± 1.4 kcal/mol and $T\Delta S^{\ddagger}_{25}$ = 8.2 ± 1.4 kcal/mol.

Table 2: Thermodynamic Values Describing Binding and Reduction of DHF and DHP by R67 DHFR Monitored by Steady-State Kinetics at pH 7.0, 25 °C

complex	value	ΔG (kcal/mol)	ΔH (kcal/mol)	$T\Delta S$ (kcal/mol)
E·NADPH[a]	$K_{d(NADPH)} = 2.8\ \mu M$	−7.5	−8.6	−1.1
E·NADPH·DHF[b]	$K_{m(DHF)} = 2.4\ \mu M$	−7.7	−14.1	−6.4
[E·NADPH·DHF]$^{\neq}$	$k_{cat} = 0.77\ s^{-1}$	17.6	6.3	−11.3
E·NADPH·DHP[c]	$K_{m(DHP)} = 23\ \mu M$	−6.3	−7.5	−1.2
relative to DHF binding		$\Delta\Delta G = 1.4$	$\Delta\Delta H = 6.6$	$\Delta(T\Delta S) = 5.2$
[E·NADPH·DHP]$^{\neq}$	$k_{cat} = 4.9 \times 10^{-4}\ s^{-1}$	22.0	13.7	−8.3
relative to DHF reduction		$\Delta\Delta G = 4.4$	$\Delta\Delta H = 7.4$	$\Delta(T\Delta S) = 3.0$

[a] For comparison, ITC values describing binding of NADPH at 28 °C, pH 8, are $K_d = 2.5\ \mu M$, $\Delta G = -7.7$ kcal/mol, $\Delta H = -8.6$ kcal/mol, $T\Delta S = -0.9$ kcal/mol (*6*). [b] For comparison, ITC values describing binding of DHF to R67 DHFR·NADP$^+$ at 25 °C, pH 8, are $K_d = 1.6\ \mu M$, $\Delta G = -7.9$ kcal/mol, $\Delta H = -13.3$ kcal/mol, $T\Delta S = -5.4$ kcal/mol (Table 1). ITC experiments are performed at pH 8 rather than pH 7 to minimize any contribution to the enthalpy change from the pH-dependent tetramer to 2 dimers dissociation (*2*). [c] For comparison, ITC values describing binding of DHP to R67 DHFR·NADP$^+$ at 25 °C, pH 8, are $K_d = 18.3 \pm 0.5\ \mu M$, $\Delta G = -6.5 \pm 0.1$ kcal/mol, $\Delta H = -9.5 \pm 0.2$ kcal/mol, $T\Delta S = -3.0 \pm 0.2$ kcal/mol.

existed for the pABA-glu tail−K32 interaction, then the asymmetric mutants would have shown different behavior (*20*). These various studies, combined with the present viscosity studies, support a role for water in binding of DHF. We have previously proposed solvent-separated ion pairs (*52*−*56*) may exist between the glu tail of DHF and K32 residues in R67 DHFR (*20*, *57*). Solvent-separated ion pairs would also diminish the desolvation penalty involved in binding (*58*). Water-stabilized binding has also been seen in an antibody−lysozyme interaction (*59*), as well as ligand binding to adenosine deaminase (60).

Comparison of Enthalpies Derived from Temperature-Dependent Kinetic Studies and ITC. Previously, a strong preference for initial binding of NADPH to R67 DHFR, followed by binding of DHF, has been proposed based on the relative K_d values, as well as the behavior of site-directed mutants (*6*, *20*). This preferred binding mechanism will be used here as well. The enthalpy change associated with binding NADPH was found to be -8.6 ± 0.6 kcal/mol using a van't Hoff approach. This value compares well with a ΔH of -8.6 ± 0.2 kcal/mol previously monitored by ITC at 28 °C (*6*), indicating the two approaches converge to similar answers.

The enthalpy change associated with formation of the R67 DHFR·NADPH·DHF complex from R67 DHFR·NADPH can be estimated by monitoring the temperature dependence of $1/K_{m(DHF)}$. The value obtained is -14.1 ± 0.6 kcal/mol. This figure compares well with an ITC-derived ΔH value of -13.3 ± 0.9 kcal/mol describing binding of DHF to R67 DHFR·NADP$^+$ (25 °C, Table 1). While the latter is a product−substrate complex, the convergence of the ΔH values (from ITC and Arrhenius plots) suggests it is a reasonable mimic of the productive ternary complex.

Construction of a Gibbs Free Energy Diagram. Combining the above ΔG and ΔH values as well as values obtained from the Arrhenius plot describing k_{cat} allows construction of a Gibbs free energy diagram at 25 °C. The resulting plot is shown in Figure 5. Formation of the binary and ternary complexes is clearly enthalpy-driven, while formation of the transition state contains a large entropic contribution.

Jencks has suggested large entropic components can be associated with enzyme catalysis, particularly those describing bisubstrate reactions (*61*, *62*). However, previous studies have found wide distributions of enthalpy and entropy terms can be associated with k_{cat}. As examples of bisubstrate reactions, (a) for peptide bond formation in the ribosome, $\Delta G^{\ddagger} = 16.5$ kcal/mol, $\Delta H^{\ddagger} = 17.2$ kcal/mol, and $T\Delta S^{\ddagger} = 0.7$ kcal/mol (*63*); (b) for truncated ATP sulfurylase from *Penicillium chrysogenum*, a $\Delta G^{\ddagger}$ value of 17.4 kcal/mol was calculated as well as a $\Delta H^{\ddagger}$ value of 16.3 kcal/mol with a $T\Delta S^{\ddagger}$ value of −1.1 kcal/mol (at 30°C and where the rate-determining step describes catalysis of the ternary substrate complex to the ternary product complex coupled with Mg-pyrophosphate release) (*64*); (c) for thymidylate synthetase, a $\Delta G^{\ddagger}$ value of 10.6 kcal/mol describing the hydride transfer rate was determined with a $\Delta H^{\ddagger}$ of 3.4 and a corresponding $T\Delta S^{\ddagger}$ of −7.2 kcal/mol (*65*); and (d) for the catalytic antibody 29G12 catalyzing a 1,3-dipolar cycloaddition reaction, a $\Delta G^{\ddagger}$ value of 17.7 kcal/mol with a $\Delta H^{\ddagger}$ of 7.1 and a $T\Delta S^{\ddagger}$ of −10.6 kcal/mol were observed (*66*).

As noted above, our Arrhenius data describing R67 DHFR catalysis indicate that $\Delta G^{\ddagger}$ is dominated by the entropy term. Typically, positive $\Delta S^{\ddagger}$ values are associated with reorganization of solvent (*67*−*69*), while studies with ordered water molecules in active sites suggest entropic values can be negative but coupled with an approximately equal ΔH contribution ((*70*, *71*) and references therein). Negative $\Delta S^{\ddagger}$ terms typically describe loss of translational and rotational motion in the transition state (*1*). Since crystal structure and NMR data indicate minimal motion of R67 DHFR upon ligand binding (*4*, *72*), changes in ligand orientation are more likely to describe the large, negative entropic term in R67 DHFR. Additionally, when substrates become more charged in their transition states (as is likely in DHFR with DHF protonated at N5), $\Delta S^{\ddagger}$ is usually negative. Thus, many factors could be involved in this large, negative $\Delta S^{\ddagger}$ term.

Typical hydride transfer reactions have enthalpies of activation near 8−15 kcal/mol (*73*). However, activation energies of 11.9, 5.5, and 3.7 kcal/mol have been calculated for chromosomal DHFRs from *Thermotoga maritima* (*74*), *Bacillus stearothermophilus* (*75*), and *E. coli* (*76*). The *E. coli* chromosomal DHFR value was obtained at pH 9.0 where the hydride transfer rate is rate-determining (*77*). At pH 9, its $\Delta G^{\ddagger}_{25}$, $\Delta H^{\ddagger}_{25}$, and $T\Delta S^{\ddagger}_{25}$ values are 16.0, 3.1, and −12.9 kcal/mol, respectively. These values are near those observed for R67 DHFR, indicating the same general range

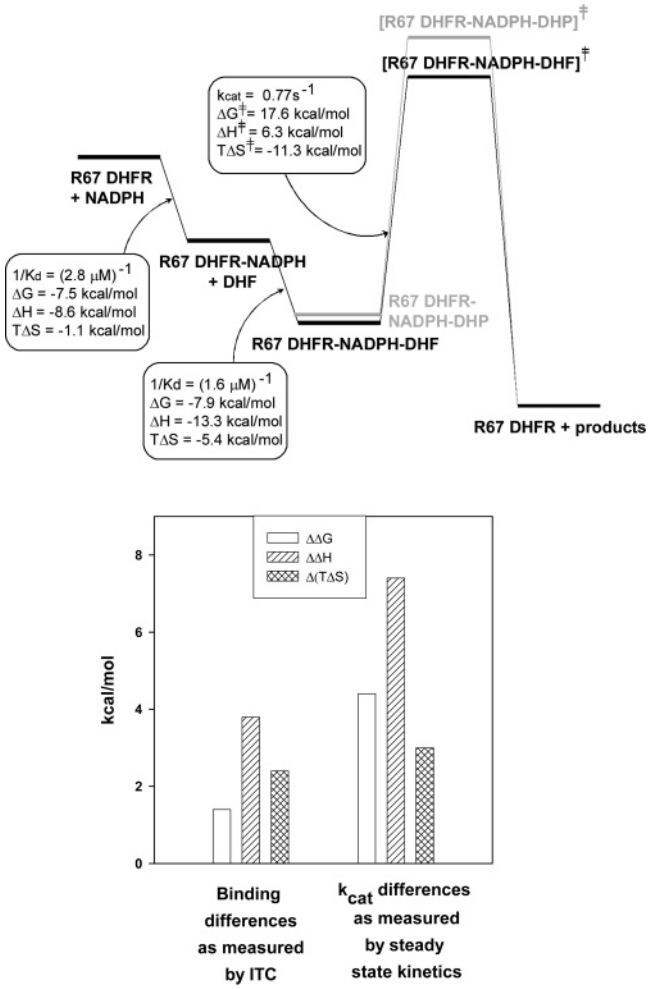

FIGURE 5: A Gibbs free energy diagram describing R67 DHFR catalysis at 25 °C. The ΔG values for DHF reduction were obtained from the observed $K_{d(NADPH)}$, $K_{d(DHF)}$, and k_{cat} values and are shown in black. The enthalpic contributions were calculated as described in the text. Since $K_{m(DHF)}$ could possibly contain kinetic terms, the K_d for DHF binding to R67 DHFR·NADP$^+$ was used to mimic productive ternary complex formation. Use of the poor substrate, DHP, is shown in gray. The bottom panel shows a bar graph depicting the differences between DHF and DHP binding and reduction describing $\Delta\Delta G$, $\Delta\Delta H$, and $\Delta(T\Delta S)$ terms. The binding differences were calculated using ITC data for formation of R67 DHFR·NADP$^+$·DHF and R67 DHFR·NADP$^+$·DHP at 25 °C, pH 8 (*57*). ITC experiments were performed at pH 8 rather than pH 7 to minimize any contribution to the enthalpy change from the pH-dependent tetramer to 2 dimers dissociation (*2*).

for these reactions. The similarity of these values is likely coincidence, as chromosomal and R67 DHFRs have entirely different structures, active sites, and transition states (*5*, *7*, *23*, *24*).

Finally, use of DHP as an alternate substrate only weakens binding by 10-fold with respect to DHF. Previous studies found the glutamic acid moiety of the pABA-glu tail provides most of the enthalpic signal associated with DHF binding (*57*); thus, substitution of glutamate by a carboxylate group weakens the enthalpic contribution. $\Delta\Delta H$ values of 3.8 or 6.5 kcal/mol can be calculated when ITC values or the slopes in the Arrhenius plots describing $1/K_m$ for DHF versus DHP binding are compared, respectively. This $\Delta\Delta H$ range supports binding tightness as playing a large role in the decrease in k_{cat}. For catalysis, a $\Delta\Delta H$ of 7.6 kcal/mol is observed (compared to DHF reduction). These results strongly implicate the pABA-glu tail in correctly docking DHF in the active site pore pursuant to catalysis. Also, when considering the terms in the equation $\Delta\Delta G = \Delta\Delta H - \Delta(T\Delta S)$, a greater contribution from $\Delta\Delta H$ can be observed, indicating partial entropic compensation (*45*). These results all suggest increases in the range of motion associated with bound DHP could interfere with catalysis.

Does Protonation Play a Role? Another possible interpretation of the thermodynamic values for R67 DHFR arises if protonation and hydride transfer are concerted events. To address this issue, the question of how DHF is protonated in the R67 DHFR active site needs consideration first. In one scenario, the predominant species, neutral DHF would bind and then be protonated. Alternatively, R67 DHFR could preferentially bind protonated DHF (HDHF). However, this species is at an extremely low concentration at pH 7. Since the N5 pK_a = 2.60 (extrapolated to 25 °C), the ratio of DHF to HDHF can be calculated as 2.5×10^4 at pH 7. If protonated DHF is the actual substrate, then the observed K_m is an apparent value. A K_m of 96 pM for protonated DHF can be calculated by dividing the apparent K_m by the HDHF concentration (*78*). If productive binding of substrate in R67 DHFR indeed utilizes the protonated species, the observed DHF K_m would be expected to decrease as the concentration of HDHF increases (i.e., decreasing pH). However, in our H62C mutant,[4] the reverse is observed, as the $K_{m(DHF)}$ rises going from pH 7 to 5 (*14*). As other ionizations could be occurring that affect K_m, the issue remains unresolved.

To estimate whether the thermodynamic values associated with protonation of DHF at N5 are at all near the catalytic thermodynamic parameters, a plot of inverse temperature versus ln K_a of the ionization constant was constructed (*79*). While this plot only contains three data points (see Supporting Information), it allows estimation of a ΔH value for N5 protonation of 6.5 ± 1.0 kcal/mol. Assuming a heat capacity of zero, extrapolation to 25 °C allows calculation of a pK_a equal to 2.60. The corresponding ΔG_{25} value is 3.6 kcal/mol with a $T\Delta S_{25}$ of 2.9 kcal/mol. While the local environment could alter the thermodynamic values associated with protonation of free versus enzyme-bound DHF (*79*, *80*), a comparison of the DHF protonation values with the values associated with k_{cat} suggests the enthalpy change associated with substrate protonation could play a role in transition-state formation if protonation and hydride transfer are concerted events. However, the entropic term for DHF protonation is positive, so this term would fight against the negative value observed during catalysis, leaving the question of whether protonation and hydride transfer are concerted unresolved. Solvent isotope effects could allow further analysis of this possibility.

Conclusion. In our present studies, as well as our ITC binding studies (*6*), R67 DHFR uses enthalpic interactions to form its NADPH·DHF complex. However, because R67 DHFR uses a "one site fits both approach" whereby both ligands are accommodated by a generalized binding surface, this binding is not optimal (*13*, *22*). Thus, it seems likely that some adjustment of the complex position and/or orienta-

[4] Wild-type R67 DHFR dissociates into inactive dimers as the pH is decreased due to protonation of His62 at the dimer−dimer interfaces (*2*). To cross-link the dimers together and be able to monitor catalysis at pH < 6.5, disulfide bonds were introduced by the H62C mutation.

tion is necessary to reach the transition state, which could be reflected by the $T\Delta S^{\ddagger}$ value of −11.3 kcal/mol. In general, both the 222 symmetry and large active site exposed to solvent support nonoptimal binding or a loose ground state. In addition, previous steady-state studies in the presence of increasing salt concentrations found that k_{cat} increased (*81*). This surprising observation suggested that a salt-sensitive interaction needed to be broken to reach the transition state, again consistent with a large entropic contribution associated with transition-state formation.

ACKNOWLEDGMENT

We thank Mark Dadmun for the use of his viscometer. We also thank Amnon Kohen, Jian Feng, and Cynthia Peterson for their helpful comments and reading of the manuscript.

SUPPORTING INFORMATION AVAILABLE

A titration showing determination of the N5 pK_a value for dihydrofolate from absorbance measurements at 20 °C, an ITC titration describing binding of DHF to R67 DHFR−$NADP^+$ to form a ternary complex in 0.75 M sucrose, and finally, a van't Hoff plot describing protonation of the N5 atom in DHF. This material is available free of charge via the Internet at http://pubs.acs.org.

REFERENCES

1. Anslyn, E. V., and Dougherty, D. A. (2006) *Modern Physical Organic Chemistry*, University Science Books, Sausalito, CA.
2. Nichols, R., Weaver, C. D., Eisenstein, E., Blakley, R. L., Appleman, J., Huang, T. H., Huang, F. Y., and Howell, E. E. (1993) Titration of histidine 62 in R67 dihydrofolate reductase is linked to a tetramer to two-dimers equilibrium, *Biochemistry 32*, 1695−706.
3. Fierke, C. A., Kuchta, R. D., Johnson, K. A., and Benkovic, S. J. (1987) Implications for enzymic catalysis from free-energy reaction coordinate profiles, *Cold Spring Harbor Symp. Quant. Biol. 52*, 631−638.
4. Narayana, N., Matthews, D. A., Howell, E. E., and Nguyen-huu, X. (1995) A plasmid-encoded dihydrofolate reductase from trimethoprim-resistant bacteria has a novel D2-symmetric active site, *Nat. Struct. Biol. 2*, 1018−1025.
5. Howell, E. E. (2005) Searching sequence space: two different approaches to dihydrofolate reductase catalysis, *ChemBioChem 6*, 590−600.
6. Bradrick, T. D., Beechem, J. M., and Howell, E. E. (1996) Unusual binding stoichiometries and cooperativity are observed during binary and ternary complex formation in the single active pore of R67 dihydrofolate reductase, a D2 symmetric protein, *Biochemistry 35*, 11414−11424.
7. Li, D., Levy, L. A., Gabel, S. A., Lebetkin, M. S., DeRose, E. F., Wall, M. J., Howell, E. E., and London, R. E. (2001) Interligand Overhauser effects in type II dihydrofolate reductase, *Biochemistry 40*, 4242−4252.
8. Smiley, R. D., Stinnett, L. G., Saxton, A. M., and Howell, E. E. (2002) Breaking symmetry: mutations engineered into R67 dihydrofolate reductase, a D2 symmetric homotetramer possessing a single active site pore, *Biochemistry 41*, 15664−15675.
9. Strader, M. B., Chopra, S., Jackson, M., Smiley, R. D., Stinnett, L., Wu, J., and Howell, E. E. (2004) Defining the binding site of homotetrameric R67 dihydrofolate reductase and correlating binding enthalpy with catalysis, *Biochemistry 43*, 7403−7412.
10. Calderone, C. T., and Williams, D. H. (2001) An enthalpic component in cooperativity: the relationship between enthalpy, entropy, and noncovalent structure in weak associations, *J. Am. Chem. Soc. 123*, 6262−6267.
11. Williams, D. H., Stephens, E., and Zhou, M. (2003) How can enzymes be so efficient? *Chem. Commun.*, 1973−1976.
12. Williams, D. H., Stephens, E., and Zhou, M. (2003) Ligand binding energy and catalytic efficiency from improved packing within receptors and enzymes, *J. Mol. Biol. 329*, 389−399.
13. Strader, M. B., Smiley, R. D., Stinnett, L. G., VerBerkmoes, N. C., and Howell, E. E. (2001) Role of S65, Q67, I68, and Y69 residues in homotetrameric R67 dihydrofolate reductase, *Biochemistry 40*, 11344−11352.
14. Park, H., Zhuang, P., Nichols, R., and Howell, E. E. (1997) Mechanistic studies of R67 dihydrofolate reductase. Effects of pH and an H62C mutation, *J. Biol. Chem. 272*, 2252−2258.
15. Marijuan, P. C. (1996) 'Gloom in the society of enzymes': on the nature of biological information, *BioSystems 38*, 163−171.
16. Blundell, T. L., and Srinivasan, N. (1996) Symmetry, stability, and dynamics of multidomain and multicomponent protein systems, *Proc. Natl. Acad. Sci. U.S.A. 93*, 14243−14248.
17. Goodsell, D. S., and Olson, A. J. (2000) Structural symmetry and protein function, *Annu. Rev. Biophys. Biomol. Struct. 29*, 105−153.
18. Kitov, P. I., and Bundle, D. R. (2003) On the nature of the multivalency effect: a thermodynamic model, *J. Am. Chem. Soc. 125*, 16271−16284.
19. Kortt, A. A., Dolezal, O., Power, B. E., and Hudson, P. J. (2001) Dimeric and trimeric antibodies: high avidity scFvs for cancer targeting, *Biomol. Eng. 18*, 95−108.
20. Hicks, S. N., Smiley, R. D., Stinnett, L. G., Minor, K. H., and Howell, E. E. (2004) Role of Lys-32 residues in R67 dihydrofolate reductase probed by asymmetric mutations, *J. Biol. Chem. 279*, 46995−47002.
21. Stinnett, L. G., Smiley, R. D., Hicks, S. N., and Howell, E. E. (2004) "Catch 222," the effects of symmetry on ligand binding and catalysis in R67 dihydrofolate reductase as determined by mutations at Tyr-69, *J. Biol. Chem. 279*, 47003−47009.
22. Howell, E. E., Shukla, U., Hicks, S. N., Smiley, R. D., Kuhn, L. A., and Zavodszky, M. I. (2001) One site fits both: a model for the ternary complex of folate + NADPH in R67 dihydrofolate reductase, a D2 symmetric enzyme, *J. Comput.-Aided Mol. Des. 15*, 1035−1052.
23. Andres, J., Moliner, V., Safont, B. S., Domingo, L. R., Picher, M. T., and Krechl, J. (1996) On transition structures for hydride transfer step: a theoretical study of the reaction catalyzed by dihydrofolate reductase enzyme, *Bioorg. Chem. 24*, 10−18.
24. Castillo, R., Andres, J., and Moliner, V. (1999) Catalytic mechanism of dihydrofolate reductase enzyme. A combined quantum-mechanical/molecular-mechanical characterizaton of transition state structure for the hydride transfer step, *J. Am. Chem. Soc. 121*, 12140−12147.
25. Tartof, K., and Hobbs, C. (1987) Improved media for growing plasmid and cosmid clones, *Bethesda Res. Lab. Focus 9*, 12.
26. Reece, L. J., Nichols, R., Ogden, R. C., and Howell, E. E. (1991) Construction of a synthetic gene for an R-plasmid-encoded dihydrofolate reductase and studies on the role of the N-terminus in the protein, *Biochemistry 30*, 10895−10904.
27. Gornall, A. G., Bardawill, C. J., and David, M. M. (1949) Determination of serum proteins by means of the biuret reaction, *J. Biol. Chem. 177*, 751−766.
28. Zhuang, P., Yin, M., Holland, J. C., Peterson, C. B., and Howell, E. E. (1993) Artificial duplication of the R67 dihydrofolate reductase gene to create protein asymmetry: effects on protein activity and folding, *J. Biol. Chem. 268*, 22672−22679.
29. Ellis, K. J., and Morrison, J. F. (1982) Buffers of constant ionic strength for studying pH-dependent processes, *Methods Enzymol. 87*, 405−426.
30. Dunn, S. M., Lanigan, T. M., and Howell, E. E. (1990) Dihydrofolate reductase from *Escherichia* coli: probing the role of aspartate-27 and phenylalanine-137 in enzyme conformation and the binding of NADPH, *Biochemistry 29*, 8569−8576.
31. Howell, E. E., Warren, M. S., Booth, C. L., Villafranca, J. E., and Kraut, J. (1987) Construction of an altered proton donation mechanism in *Escherichia coli* dihydrofolate reductase, *Biochemistry 26*, 8591−8598.
32. Smiley, R. D., Saxton, A. M., Jackson, M. J., Hicks, S. N., Stinnett, L. G., and Howell, E. E. (2004) Nonlinear fitting of bisubstrate enzyme kinetic models using SAS computer software: application to R67 dihydrofolate reductase, *Anal. Biochem. 334*, 204−206.
33. Prabhu, V., Lui, H., and King, J. (1997) *Arabidopsis* dihydropteroate synthase: general properties and inhibition by reaction product and sulfonamides, *Phytochemistry 45*, 23−27.

34. Baccanari, D., Phillips, A., Smith, S., Sinski, D., and Burchall, J. (1975) Purification and properties of *Escherichia coli* dihydrofolate reductase, *Biochemistry 14*, 5267−5273.
35. Segel, I. H. (1975) *Enzyme Kinetics: Behavior and Analysis of Rapid Equilibrium and Steady-State Enzyme Systems*, John Wiley and Sons, New York.
36. Maharaj, G., Selinsky, B. S., Appleman, J. R., Perlman, M., London, R. E., and Blakley, R. L. (1990) Dissociation constants for dihydrofolic acid and dihydrobiopterin and implications for mechanistic models for dihydrofolate reductase, *Biochemistry 29*, 4554−4560.
37. Fersht, A. (1985) *Enyzme Structure and Mechanism*, W. H. Freeman and Company, New York.
38. Wiseman, T., Williston, S., Brandts, J. F., and Lin, L. N. (1989) Rapid measurement of binding constants and heats of binding using a new titration calorimeter, *Anal. Biochem. 179*, 131−137.
39. Hegde, S. S., Dam, T. K., Brewer, C. F., and Blanchard, J. S. (2002) Thermodynamics of aminoglycoside and acyl-coenzyme A binding to the *Salmonella enterica* AAC(6′)-Iy aminoglycoside *N*-acetyltransferase, *Biochemistry 41*, 7519−7527.
40. Heyduk, E., Baichoo, N., and Heyduk, T. (2001) Interaction of the alpha-subunit of *Escherichia coli* RNA polymerase with DNA: rigid body nature of the protein-DNA contact, *J. Biol. Chem. 276*, 44598−44603.
41. Laidler, K. J., and Peterman, B. F. (1979) Temperature effects in enzyme kinetics, *Methods Enzymol. 63*, 234−257.
42. Wolfenden, R. (1999) Conformational aspects of inhibitor design: enzyme−substrate interactions in the transition state, *Bioorg. Med. Chem. 7*, 647−652.
43. Bienvenue, D. L., Mathew, R. S., Ringe, D., and Holz, R. C. (2002) The aminopeptidase from *Aeromonas proteolytica* can function as an esterase, *J. Biol. Inorg. Chem. 7*, 129−135.
44. Perrin, D., Dempsey, B., and Serjeant, E. (1981) *pK$_a$ Prediction for Organic Acids and Bases*, Chapman and Hall, London.
45. Snider, M. J., Gaunitz, S., Ridgway, C., Short, S. A., and Wolfenden, R. (2000) Temperature effects on the catalytic efficiency, rate enhancement, and transition state affinity of cytidine deaminase, and the thermodynamic consequences for catalysis of removing a substrate "anchor", *Biochemistry 39*, 9746−9753.
46. Sampson, N. S., and Knowles, J. R. (1992) Segmental motion in catalysis: investigation of a hydrogen bond critical for loop closure in the reaction of triosephosphate isomerase, *Biochemistry 31*, 8488−8494.
47. Radzicka, A., and Wolfenden, R. (1995) A proficient enzyme, *Science 267*, 90−93.
48. Mattei, P., Kast, P., and Hilvert, D. (1999) *Bacillus subtilis* chorismate mutase is partially diffusion-controlled, *Eur. J. Biochem. 261*, 25−32.
49. Feng, L., Li, Y., and Kirsch, J. F. (1998) Genetic engineering approaches to enzyme design and mechanism, *J. Phys. Org. Chem. 11*, 536−539.
50. Jelesarov, I., and Bosshard, H. R. (1994) Thermodynamics of ferredoxin binding to ferredoxin:NADP+ reductase and the role of water at the complex interface, *Biochemistry 33*, 13321−13328.
51. Alonso, H., Gillies, M. B., Cummins, P. L., Bliznyuk, A. A., and Gready, J. E. (2005) Multiple ligand-binding modes in bacterial R67 dihydrofolate reductase, *J. Comput.-Aided Mol. Des. 19*, 165−187.
52. Roca, M., Marti, S., Andres, J., Moliner, V., Tunon, I., Bertran, J., and Williams, I. H. (2003) Theoretical modeling of enzyme catalytic power: analysis of "cratic" and electrostatic factors in catechol *O*-methyltransferase, *J. Am. Chem. Soc. 125*, 7726−7737.
53. Umezurike, G. M. (1987) The mechanism of action of beta-glucosidase from *Botryodiplodia theobromae* Pat, *Biochem. J. 241*, 455−462.
54. Bagnol, L., Horner, J. H., and Newcomb, M. (2003) Direct detection of ion pair formation and collapse in a migration reaction of a beta-phosphate radical, *Org. Lett. 5*, 5055−5058.
55. Dougherty, R. C., and Howard, L. N. (2003) Analysis of excess Gibbs energy of electrolyte solutions: a new model for aqueous solutions, *Biophys. Chem. 105*, 269−278.
56. Harder, S., Feil, F., and Repo, T. (2002) "Alkaline-earth metals in a box": structures of solvent-separated ion pairs, *Chem.−Eur. J. 8*, 1991−1999.
57. Jackson, M., Chopra, S., Smiley, R. D., Maynord, P. O., Rosowsky, A., London, R. E., Levy, L., Kalman, T. I., and Howell, E. E. (2005) Calorimetric studies of ligand binding in R67 dihydrofolate reductase, *Biochemistry 44*, 12420−12433.
58. Chong, L. T., Dempster, S. E., Hendsch, Z. S., Lee, L. P., and Tidor, B. (1998) Computation of electrostatic complements to proteins: a case of charge stabilized binding, *Protein Sci. 7*, 206−210.
59. Bhat, T. N., Bentley, G. A., Boulot, G., Greene, M. I., Tello, D., Dall'Acqua, W., Souchon, H., Schwarz, F. P., Mariuzza, R. A., and Poljak, R. J. (1994) Bound water molecules and conformational stabilization help mediate an antigen−antibody association, *Proc. Natl. Acad. Sci. U.S.A. 91*, 1089−1093.
60. Dzingeleski, G. D., and Wolfenden, R. (1993) Hypersensitivity of an enzyme reaction to solvent water, *Biochemistry 32*, 9143−9147.
61. Page, M. I., and Jencks, W. P. (1971) Entropic contributions to rate accelerations in enzymic and intramolecular reactions and the chelate effect, *Proc. Natl. Acad. Sci. U.S.A. 68*, 1678−1683.
62. Jencks, W. P. (1975) Binding energy, specificity, and enzymic catalysis: the Circe effect, *Adv. Enzymol. Relat. Areas Mol. Biol. 43*, 219−410.
63. Sievers, A., Beringer, M., Rodnina, M. V., and Wolfenden, R. (2004) The ribosome as an entropy trap, *Proc. Natl. Acad. Sci. U.S.A. 101*, 7897−7901.
64. Hanna, E., Ng, K. F., MacRae, I. J., Bley, C. J., Fisher, A. J., and Segel, I. H. (2004) Kinetic and stability properties of *Penicillium chrysogenum* ATP sulfurylase missing the C-terminal regulatory domain, *J. Biol. Chem. 279*, 4415−4424.
65. Agrawal, N., Hong, B., Mihai, C., and Kohen, A. (2004) Vibrationally enhanced hydrogen tunneling in the *Escherichia coli* thymidylate synthase catalyzed reaction, *Biochemistry 43*, 1998−2006.
66. Toker, J. D., Tremblay, M. R., Yli-Kauhaluoma, J., Wentworth, A. D., Zhou, B., Wentworth, P., Jr., and Janda, K. D. (2005) Exploring the scope of the 29G12 antibody catalyzed 1,3-dipolar cycloaddition reaction, *J. Org. Chem. 70*, 7810−7815.
67. Houck, W. J., and Pollack, R. M. (2003) Activation enthalpies and entropies for the microscopic rate constants of acetate-catalyzed isomerization of 5-androstene-3, 17-dione, *J. Am. Chem. Soc. 125*, 10206−10212.
68. Jen-Jacobson, L., Engler, L. E., and Jacobson, L. A. (2000) Structural and thermodynamic strategies for site-specific DNA binding proteins, *Struct. Folding Des. 8*, 1015−23.
69. Jelesarov, I., and Bosshard, H. R. (1999) Isothermal titration calorimetry and differential scanning calorimetry as complementary tools to investigate the energetics of biomolecular recognition, *J. Mol. Recognit. 12*, 3−18.
70. Phillips, R. S. (2002) How does active site water affect enzymatic stereorecognition? *J. Mol. Catal. B: Enzym. 19−20*, 103−107.
71. Holdgate, G. A., Tunnicliffe, A., Ward, W. H., Weston, S. A., Rosenbrock, G., Barth, P. T., Taylor, I. W., Pauptit, R. A., and Timms, D. (1997) The entropic penalty of ordered water accounts for weaker binding of the antibiotic novobiocin to a resistant mutant of DNA gyrase: a thermodynamic and crystallographic study, *Biochemistry 36*, 9663−9673.
72. Pitcher, W. H., III, DeRose, E. F., Mueller, G. A., Howell, E. E., and London, R. E. (2003) NMR studies of the interaction of a type II dihydrofolate reductase with pyridine nucleotides reveal unexpected phosphatase and reductase activity, *Biochemistry 42*, 11150−11160.
73. Kohen, A., and Klinman, J. P. (1998) Enzyme catalysis: beyond classical paradigms, *Acc. Chem. Res. 31* 397−404.
74. Maglia, G., and Allemann, R. K. (2003) Evidence for environmentally coupled hydrogen tunneling during dihydrofolate reductase catalysis, *J. Am. Chem. Soc. 125*, 13372−13373.
75. Kim, H. S., Damo, S. M., Lee, S. Y., Wemmer, D., and Klinman, J. P. (2005) Structure and hydride transfer mechanism of a moderate thermophilic dihydrofolate reductase from *Bacillus stearothermophilus* and comparison to its mesophilic and hyperthermophilic homologues, *Biochemistry 44*, 11428−11439.
76. Sikorski, R. S., Wang, L., Markham, K. A., Rajagopalan, P. T., Benkovic, S. J., and Kohen, A. (2004) Tunneling and coupled motion in the *Escherichia coli* dihydrofolate reductase catalysis, *J. Am. Chem. Soc. 126*, 4778−4779.
77. Fierke, C. A., Johnson, K. A., and Benkovic, S. J. (1987) Construction and evaluation of the kinetic scheme associated with dihydrofolate reductase from *Escherichia coli*, *Biochemistry 26*, 4085−4092.
78. Schmitzer, A. R., Lepine, F., and Pelletier, J. N. (2004) Combinatorial exploration of the catalytic site of a drug-resistant dihydrofolate reductase: creating alternative functional configurations, *Protein Eng. Des. Sel. 17*, 809−819.

79. Bhattacharya, S., and Lecomte, J. T. (1997) Temperature dependence of histidine ionization constants in myoglobin, *Biophys. J. 73*, 3241−3256.
80. Sarmini, K., and Kenndler, E. (1999) Ionization constants of weak acids and bases in organic solvents, *J. Biochem. Biophys. Methods 38*, 123−137.
81. Hicks, S. N., Smiley, R. D., Hamilton, J. B., and Howell, E. E. (2003) Role of ionic interactions in ligand binding and catalysis of R67 dihydrofolate reductase, *Biochemistry 42*, 10569−10578.

BI052504L